crystals

MDPI

Article

Structural Insights into Ni(II), Cu(II), and Zn(II) Coordination Complexes of Arylazoformamide and Arylazothioformamide Ligands

Laxmi Tiwari †, Jake Nelson and Kristopher V. Waynant *

Department of Chemistry, University of Idaho, Moscow, ID 83844, USA; laxmi.tiwari2@mssm.edu (L.T.); jake9676@vandals.uidaho.edu (J.N.)
* Correspondence: kwaynant@uidaho.edu
† Current address: Icahn School of Medicine at Mount Sinai, New York, NY 10029, USA.

Abstract

Understanding how redox-active ligands coordinate to metal centers of different oxidation states is essential for applications ranging from metal remediation and recycling to drug discovery. In this study, coordination complexes of nickel(II), copper(II), and zinc(II) chloride salts were synthesized by mixing the salts with either arylazoformamide (AAF) or arylazothioformamide (ATF) ligands in toluene or methanol. The AAF and ATF ligands coordinate through their 1,3-heterodienes, N=N–C=O and N=N–C=S, respectively, and, due to their known strong binding, the piperidine and pyrrolidine formamide units were selected, as was the electron-donating methoxy group on the aryl ring. A total of 12 complexes were obtained, representing potential chelation events from ligand-driven oxidation of zerovalent metals and/or coordination of oxidized metal salts. The X-ray crystallography revealed a range of coordination patterns. Notably, the Cu(II)Cl_2 complexes, in the presence of ATF, produce [ATF-CuCl]$_2$ dimers, supporting a potential reduction event at the copper, while other metals with ATF and all metals with AAF remain in the 2+ oxidation state. Hirshfeld analysis was performed on all complexes, and it was found that most interactions across the complexes were dominated by H. . .H, followed by Cl. . .H/H. . .Cl, with metals showing very little to no interaction with other atoms. Spectroscopic techniques such as UV–VIS absorption, NMR (when diamagnetic), and FTIR, in addition to electrochemical studies support the metal–ligand coordination.

Keywords: coordination chemistry; 1,3-heterodiene coordination; redox-active ligands; arylazothioformamide; azoformamide

check for updates

Academic Editor: Waldemar Maniukiewicz

Received: 17 September 2025
Revised: 1 October 2025
Accepted: 1 October 2025
Published: 4 October 2025

Citation: Tiwari, L.; Nelson, J.; Waynant, K.V. Structural Insights into Ni(II), Cu(II), and Zn(II) Coordination Complexes of Arylazoformamide and Arylazothioformamide Ligands. *Crystals* **2025**, *15*, 869. https://doi.org/10.3390/cryst15100869

Copyright: © 2025 by the authors. Licensee MDPI, Basel, Switzerland. This article is an open access article distributed under the terms and conditions of the Creative Commons Attribution (CC BY) license (https://creativecommons.org/licenses/by/4.0/).

1. Introduction

Metal complexes have widespread applications in catalysis and materials science, as well as in drug development and medicinal chemistry [1–3]. Transition metals such as Ni(II), Cu(II), and Zn(II) with partially filled *d*-orbitals and variable oxidation states, can play a role in biological redox reactions [4–7] and are useful in catalyst design for modern synthetic organic chemistry [8,9]. Ligands and their coordination events play crucial roles in both controlling the reactivity and the stability of the metal complex [10]. Arylazothioformamides (ATFs) and arylazoformamides (AAFs), similar to thiosemicarbazone and semicarbazones, consist of 1,3-heterodiene N=N–C=S and N=N–C=O motifs, respectively [11]. ATF ligands were first reported in the late 1960s/early 1970s forming coordination complexes with late-transition metals [12–14], and, by the early 2000s, were

shown to be effective purification agents, oxidatively dissolving and removing metals from advanced polymeric materials [15,16]. AAF ligands have seen less evaluation for coordination with an example as a palladium(II)-bound ligand for Suzuki [17] and Sonogashira reactions [18], while also having been explored for the Mitsunobu reaction [19]. These ligands, such as **1a,** have the ability to oxidatively dissolve and/or coordinate to many late-transition metals (i.e., Cu, Pd, Ni, and Zn) through a mild process, which increases their potential use in separation and/or recovery of metals from mixed-metal systems [11,20]. The synthesis and evaluation of coordination complexes formed between Ni(II), Cu(II), and Zn(II) salts with ATF or AAF ligands provide insight into the redox activity of the ligands and systems, while also revealing structural variations across different metals. The ATF and AAF ligands for this study (**1b/c** and **4a/b**) shown in Figure 1, were formed from pyrrolidine or piperidine as the secondary amine creating the thioformamide/formamide moiety and the aryl ring is *para*-substituted with the electron-donating (-OMe) group. Previously, we have found that ATF ligands with sterically locked secondary amines (i.e., pyrrolidine/piperidine) and strong electron-donating groups (i.e., -OMe) produced higher binding affinities with metal salts, creating compounds such as **3a–c** [11,21]. For this study, the coordination pattern of ATF with various metal salts was compared against each other as well as against the AAF metal complexes.

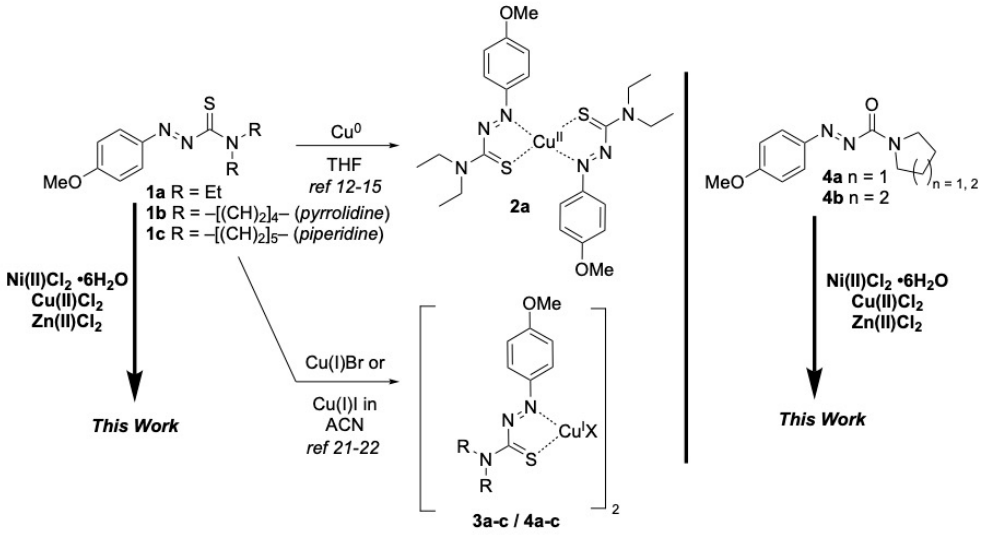


Figure 1. ATF and AAF coordination overview and basis for the current study. ATFs have seen extensive study in oxidative dissolution of zerovalent copper and coordination to copper(I) salts. Neither ATF nor AAF has seen extensive investigation with metal(II) salts.

2. Results

ATF (**1b/c**) and AAF (**4a/b**) ligands were synthesized according to our previous reports [11,17,20]. Coordination complexes were formed from the simple reflux of ATF or AAF ligands with the metal(II) chloride salts in either toluene or methanol for 4 h, as shown in Figures 2 and 3. After cooling to room temperature, the complexes precipitated and were collected and washed with hexanes to remove excess ligand. If not crystalline, they were recrystallized using slow evaporation or vapor diffusion processes using toluene or acetonitrile/ether solutions. All crystalline complexes were characterized using single crystal X-ray diffraction (XRD) with structures shown in Figures 2 and 3. Complexes **12** and **13** have been published previously, but their structures were not compared to other complexes [17,20]. XRD experimental details for complexes **5–11** and **14–16** can be found in the electronic supporting information.

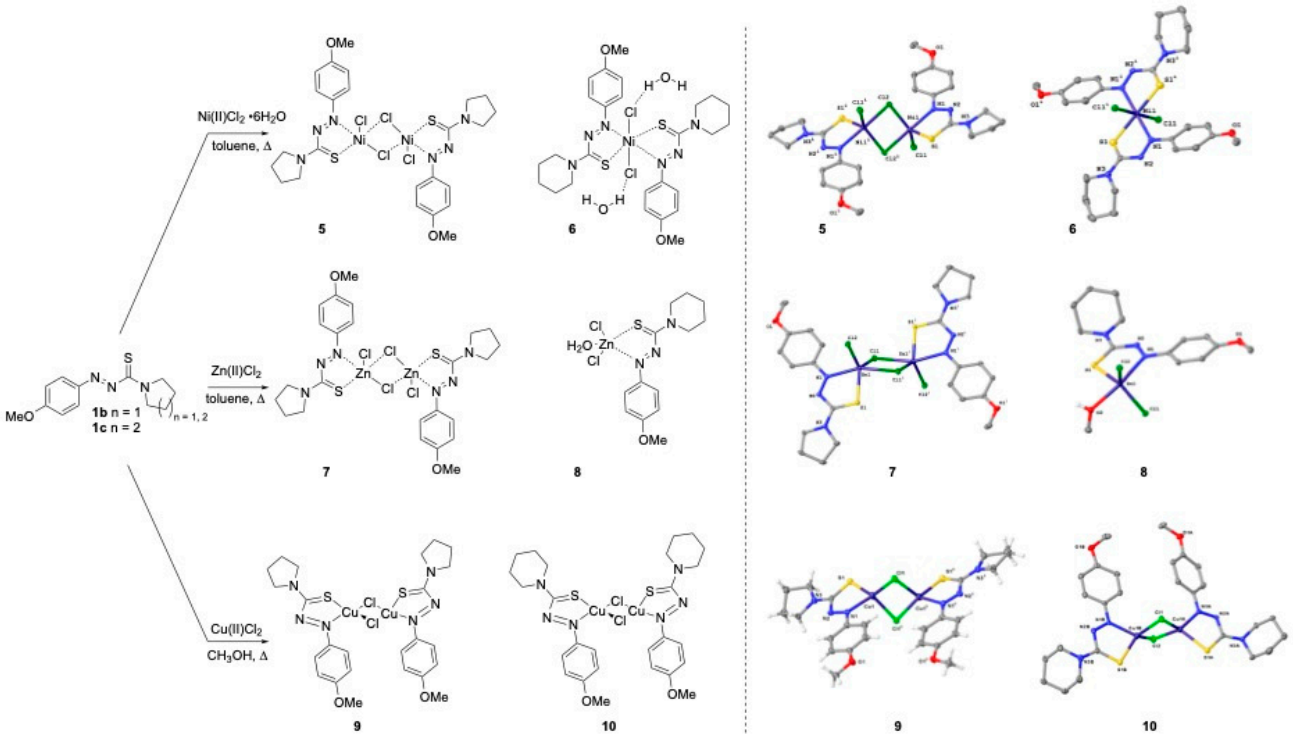


Figure 2. Metal(II) chlorides react with ATF ligands to give unique coordination complexes (**left**) as seen through their X-ray crystallographic unit cells (**right**).

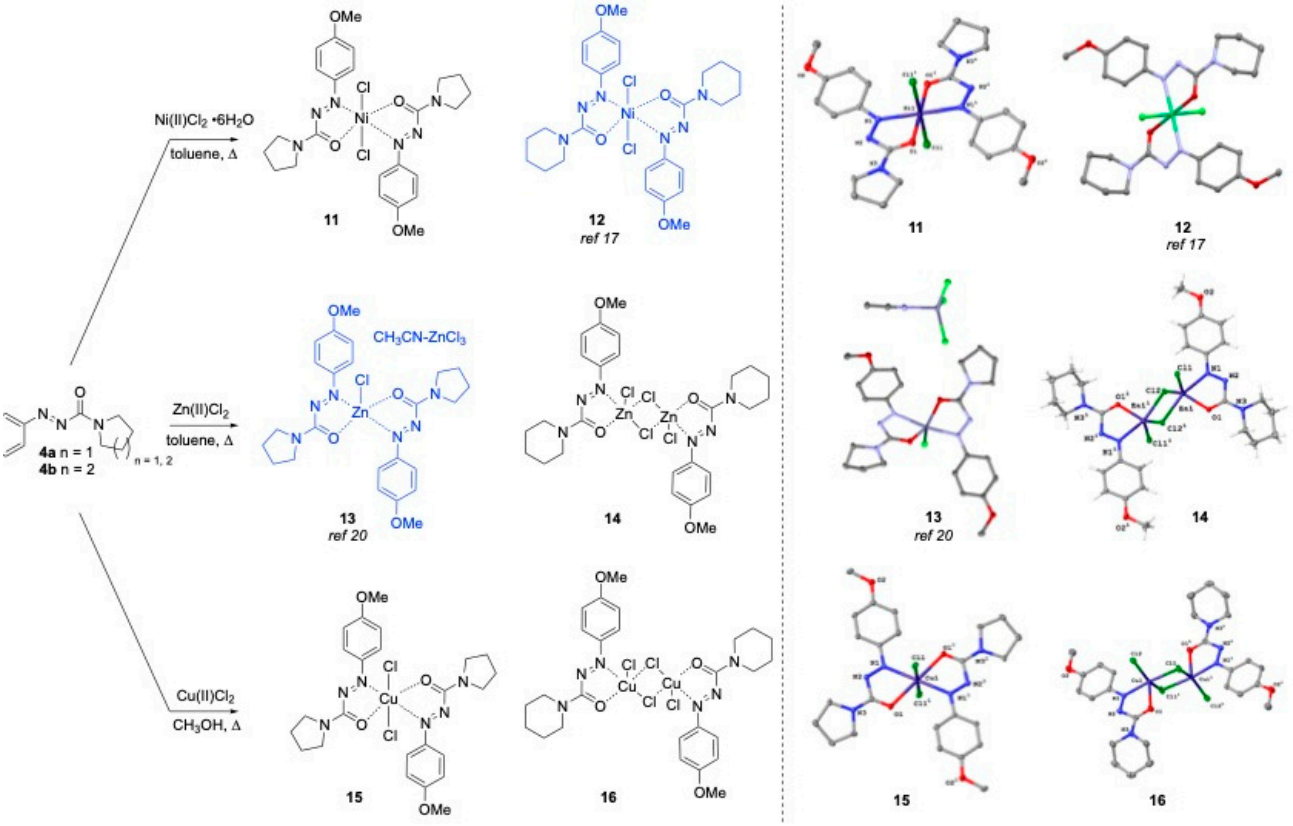


Figure 3. Metal(II) chlorides react with AAF ligands to give unique coordination complexes (**left**) as seen through their X-ray crystallographic unit cells (**right**). Complexes **12** and **13** have been reported previously [17,20].

2.1. X-Ray Crystal Structure Analysis

Single crystals suitable for diffraction were isolated for all complexes. Following toluene reflux, Ni(II)ATF **5/6** and Ni(II)AAF **11/12** complexes were obtained by vapor diffusion of diethyl ether into acetonitrile solutions. Complexes **5** and **11** appear in a monoclinic crystal system with *I2/a* and *P21/n* space groups, respectively, whereas **6** and **12** appear in a triclinic system with *P1* space group. The main difference between ATF and AAF-Ni(II) complexes is that the *pyr*-ATF-Ni(II) complex **5** contains two $NiCl_2$ molecules with two ATF ligands representing a 2:2 (1:1 dimer) coordination pattern, whereas the *pip*-ATF-Ni(II) complex **6** and both *pyr*-AAF-Ni(II) **11** and *pip*-AAF-Ni(II) **12** complexes contain one Ni(II) atom with two AAF ligands in a 1:2 metal/ligand coordination pattern with the chlorides in complex **6** each coordinating a water molecule. Zinc complexes were obtained by slow evaporation of acetonitrile or methanolic solutions. Complex **7** crystallizes in a monoclinic crystal system with the $I2/a$ (15) space group. Instead, **8** crystallizes in a triclinic crystal system with the $P\bar{1}(2)$ space groups and contains two $ZnCl_2$ compounds as a 1:1 dimer with the bidentate *pip*-AAF ligand. Complex **13**, previously reported, crystallized into an orthorhombic system with a *Pbca* (61) space group [20]. This crystal structure, from *pyr*-AAF, uniquely contains an acetonitrile trichloridozincate counterion formed during crystallization, which was not seen with the other metals nor with the *pip*-AAF zinc complex **14**. However, complex **14** also crystallizes in orthorhombic system with a *Pbca* (61) space group. Numerous attempts were made to crystallize **13** from toluene or methanol to determine if, prior to acetonitrile conjugation, the structure would mimic either its nickel(II) or copper(II) pyrrolidine congeners.

Coordination complexes of AAF and ATF from copper(II) chloride addition were obtained by the slow evaporation of acetonitrile solutions. Complexes **9** and **15** appear in a monoclinic crystal system with *C2/c (15)* and *P21/c (14)* space groups, respectively, whereas **10** and **16** adopt orthorhombic systems with $Pna2_1$ and *Pbca* (61) space groups, respectively. From the crystal structures, complexes **9** and **10** produce 2:2 (1:1 dimer) complexes with the two copper centers in distorted tetrahedrons, each binding one ATF ligand and coordinating to both chloride atoms. This suggests the copper metal has been reduced from Cu(II) to Cu(I) upon coordination with ATFs. As the yields are close to 50%, this may indicate that ligand and/or solvent was lost/decomposed, essentially oxidized, to support metal reduction. The reduction of copper(II) was also supported through ^{1}H NMR, yielding spectra that do not indicate paramagnetic species. This is not seen in complexes **15** and **16**, where the $Cu(II)Cl_2$ salts coordinate AAF either as a 2:1 system (i.e., **15**) with the axial chlorides in an octahedral arrangement or as dimeric distorted tetrahedrons (i.e., **16**) with the chlorides bridging the two copper atoms.

Complexes were analyzed for the key bond distances and bond angles in the chelation motif. Notably, both copper complexes from *pip*-ATF and *pyr*-ATF (**9** and **10**) displayed shorter Metal–N_1 (2.0614, 2.002 Å); and Metal–S_1 distances (2.2749, 2.3056 Å) than the zinc or nickel species as shown in Table 1, indicating the potential change in the oxidation state of copper(II) to copper(I). With the other possibility being the reduction of the ligands to maintain the copper(II) oxidation state, the bond distances and angles were compared to other reported copper(I)ATF species and were shown to be consistent with copper(I) [22,23]. The *pip*-AAF and *pyr*-AAF bond distances were all consistent and indicated the oxidation states remained as metal(II).

Table 1. Key bond distances (Å), bond angles, and torsion angles for the chelation in coordination complexes **5–16**.

Metal	Complex	N_1–Metal	S_1–Metal	N_1=N_2	N_2–C_1	C_1=S_1	Complex	N_1–Metal	O_1–Metal	N_1=N_2	N_2–C_1	C_1=O_1
Ni	**5**	2.1336(18)	2.2830(6)	1.269(2)	1.422(3)	1.689(2)	**11**	2.1554	2.0445	1.268(2)	1.443(2)	1.243(2)
	6	2.121(3)	2.3737(9)	1.260(4)	1.431(4)	1.668(3)	**12**	2.0949(19)	2.0366(16)	1.267(3)	1.452(3)	1.243(3)
Zn	**7**	2.3414(10)	2.3129(3)	1.2647(13)	1.4256(14)	1.6986(12)	**13**	2.207(3)	2.002(3)	1.267(4)	1.435(5)	1.256(4)
	8	2.3833(11)	2.3441(3)	1.2671(14)	1.4212(15)	1.6991(13)	**14**	2.2917(18)	2.0199(16)	1.268(2)	1.440(3)	1.250(3)
Cu	**9**	2.061(4)	2.2749(12)	1.267(5)	1.427(5)	1.688(4)	**15**	2.1813(13)	2.2915(12)	1.2628(19)	1.449(2)	1.2309(19)
	10	2.002(5)	2.3056(15)	1.267(6)	1.433(7)	1.690(5)	**16**	2.051(3)	2.186(2)	1.261(4)	1.450(4)	1.232(4)
		Bond Angles (°)			**Torsion Angles (°)**			**Bond Angles (°)**			**Torsion Angles (°)**	
Metal	**Complex**	**N_1-N_2-C_1**	**N_2-C_1-S_1**	**N_1-M-S_1**	**N_1=N_2–C_1=S_1**		**Complex**	**N_1-N_2-C_1**	**N_2-C_1-O_1**	**N_1-M-O_1**	**N_1=N_2–C_1=O_1**	
Ni	**5**	114.64(17)	124.37(15)	82.53(5)	2.7(3)		**11**	110.41(14)	123.15(15)	104.65(5)	−0.6(2)	
	6	113.9(3)	123.7(2)	80.15(7)	14.2(4)		**12**	109.37(18)	122.1(2)	103.98(7)	−9.8(3)	
Zn	**7**	114.31(10)	126.00(8)	78.84(2)	5.47(15)		**13**	110.5(3)	123.5(3)	75.27	1.0(5)	
	8	113.76(10)	124.95(9)	77.40(3)	−4.05(16)		**14**	110.45(17)	122.87(19)	72.73(6)	2.0(3)	
Cu	**9**	113.7(4)	124.8(3)	84.17(11)	−3.9(6)		**15**	112.22(13)	123.84(15)	71.55	−0.4(2)	
	10	114.1(4)	123.2(4)	84.20(14)	10.5(7)		**16**	111.7(3)	122.0(3)	74.71	−2.1(4)	

2.2. Hirshfeld Analysis of Crystal Structures

In order to understand the association between crystal structures and the physicochemical properties of ATF and AAF complexes, Hirshfeld surface plots and 2D fingerprints were explored using *Crystal Explorer 17.5* [24]. Red and blue dots on the Hirshfeld surfaces demonstrate the high and low close-contact populations, respectively, within the crystal, and these interactions are shown in Figure 4 using coordination complex **5** as an example. Hirshfeld surface analysis for complexes **6–12** and **14–16** can be found in ESI (Figure S1), with complex **13** having been previously reported [20]. The red area, in Figure 4A, which is focused on the oxygen and nitrogen, indicates intense O. . .H/H. . .O and N. . .H/H. . .O interactions. Most interactions found throughout the complexes were H. . .H, followed by Cl. . .H/H. . .Cl. All complexes indicated very low or no interaction of metals with other atoms.

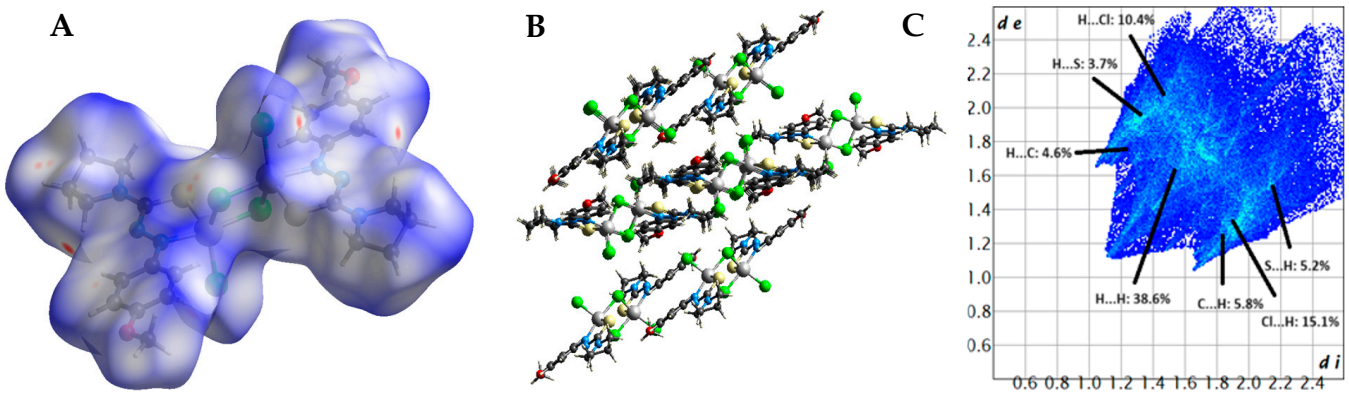


Figure 4. (**A**) Hirshfeld surface analysis, (**B**) Hirshfeld surface to visualize intermolecular interaction, and (**C**) fingerprint plot of major contacts in compound **5**.

2.3. Spectroscopic Analysis of Complexes

Spectral data of the ligands vs. that of the metal–ligand coordination complexes were compared to showcase both similarities and key differences. Particularly, UV–Vis, FTIR, and $^{1}H/^{13}C$ NMR (when possible) experiments were evaluated. The electronic spectra of the ATF and AAF ligands complexes from copper(II), nickel(II), and zinc(II) ions were recorded in acetonitrile solution at room temperature, and the data are collected in Table 2

with a spectral example in Figure 5, using copper complexes (**9**, **10**, **15**, and **16**) as examples. Nickel and zinc complexes are shown in ESI (Figures S14 and S15). The electronic spectra of the free ligands have been published previously [11] and give intense absorption maxima in the UV region at 243 and 323 for **1b** and **1c** and 235 and 324 nm for **4a** and **4b,** which are assigned to π-π* and n-π* transitions. These transitions are also found in the spectral data of the complexes but are shifted either towards lower or higher frequencies (by 5–10 nm), confirming the coordination of the ligand to the metal ions. The electronic spectra of the copper(II) complexes **9**, **10**, **15,** and **16** also show the ligand-based transitions. Cu(II) complexes are known to show LMCT transitions, and it is likely that the strong visible band features may be S/O → Cu(II) charge transfer in the region of 407–412 nm. A weak and broad, longer-wavelength band was observed in the region near 678 nm, which was assigned to a Cu(II)-centered *d*—*d* transition for complexes **15** and **16**, consistent with the previous report [25]. Similar broad bands in the 600–700 nm region are absent in **9** and **10**, suggesting the absence of, or a very weak Cu(II)-centered *d*–*d* transition and providing more evidence for copper(I).

Table 2. UV–Vis absorbance and electrochemical data for ligands and metal complexes.

Compound	λ_{max}/nm (ε/M^{-1} cm^{-1})	E_{ox} (V)	E_{red} (V)
1b	243 (25,861), 323 (29,309)	+0.73	−0.79, −1.35
1c	249 (22,413), 322 (19,482)	+0.81	−0.78, −1.30
4a	237 (11,896), 324 (15,517)	+1.27	−0.10, −1.59
4b	234 (12,069), 323 (6034)	+1.32	−1.10, −1.65
5	425 (13,965)	+0.84, +1.27	−0.09, −1.12, −1.54
6	424 (7414)	+0.77, +1.29	−0.10, −0.91, −1.42
7	423 (19,655)	+0.85, +1.46	−0.30, −1.27
8	425 (9138)	+0.77, +1.36	−0.09, −1.04, −1.41
9	412 (31,896), 679 (4655)	+0.26, +1.11	−0.54, −0.89, −1.47
10	411 (26,896), 678 (3448)	+0.29, +1.15	−0.52, −0.73
11	394 (7069)	+0.86, +1.22	−0.28
12	393 (4655)	+0.83, +1.21	−0.32
13	410 (4207)	+0.85, +1.21	−0.27
14	411 (3103)	+0.85, +1.23	−0.33
15	407 (7931)	+0.24, +1.27	−0.60, −1.07, −1.38
16	408 (14,138)	+0.26, +1.29	−0.59, −1.02, −1.40

The UV–visible spectrum of nickel(II) complexes, **5**, **6**, **11**, and **12** show absorption bands at 235–250, 320–325 nm, and 395–425 nm, respectively (Figure S14). The strong band at 235–250 nm and 320–325 nm are assigned to the ligand-centered π-π* and n-π* transition, respectively. For complexes **5** and **6**, intense bands were also observed at 425 nm, which were assigned to S → Ni(II) LMCT bands, whereas 394 nm for complexes **11** and **12** were assigned to O → Ni(II) LMCT. Nickel(II) complexes **6**, **11**, and **12** appear to be purely octahedral, and it is expected that they will show three *d*–*d* bands corresponding to $^3A_{2g} \rightarrow {}^3T_{2g}$, $^3A_{2g} \rightarrow {}^3T_{1g}$, and $^3A_{2g} \rightarrow {}^3T_{1g}$(P) transitions [26]. However, no *d*–*d* bands could be identified for the nickel(II) complexes at these low concentrations.

The electronic spectrum of zinc(II) complexes **7**, **8**, **13,** and **14** show absorbances in the range of 240–250 nm, 320–325 nm, and 410–423 nm (Figure S15). The bands at 240–250 nm and 320–325 nm are assigned as π-π* and n-π* transitions, respectively, while the band at 410–423 nm are assigned to S/O→Zn charge transfer. Interestingly, the intensity of the S→Zn charge transfer band in complex **7** was two times higher than **8** and almost five times higher than **13** and **14**.

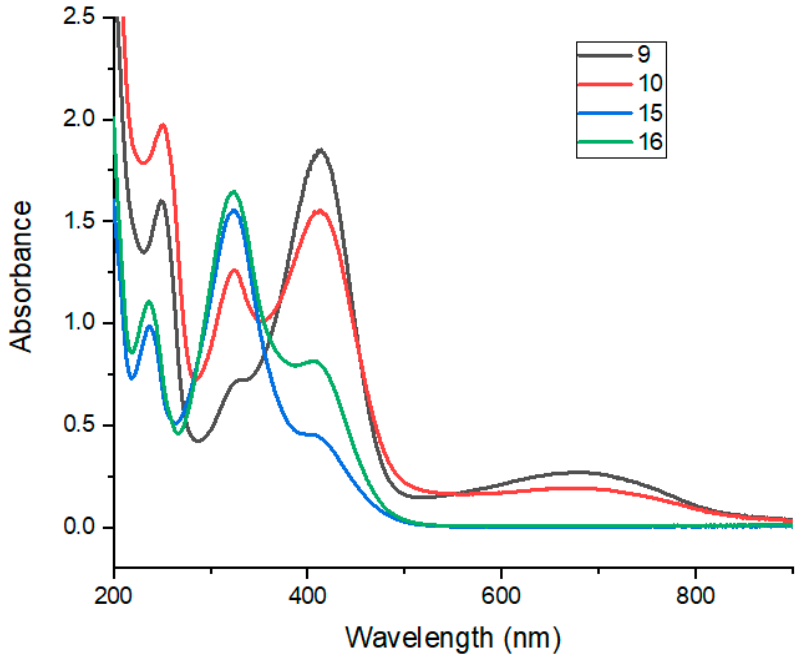


Figure 5. UV–Vis absorbance spectra of copper complexes **9**, **10**, **15**, and **16** (concentration: 5.8×10^{-5} M).

2.4. Electrochemical Studies

The electrochemical data of the ligands and complexes are given in Table 2, and a representative cyclic voltammogram of complex **14** is shown in Figure 6 (others are provided in the ESI, Figures S11–S13). Ferrocene (Fc) was used as an internal standard, and all redox potentials are referenced to the $Fc^{+/}Fc^{0}$ couple [27]. The cyclic voltammograms (CVs) of the complexes show metal-centered processes and waves corresponding to the ligand. Repeated scans, as well as different scan rates, did not indicate any sign of dissociation. The CVs of the ligands in acetonitrile exhibit an irreversible anodic wave in the positive potential range, with values of 0.73 V for ligand **1b**, 0.81 V for ligand **1c,** 1.27 V for ligand **4a**, and 1.32 V for ligand **4b** (Figure S10). Additionally, two quasi-reversible cathodic waves were observed in the negative potential range, occurring at −0.79 V and −1.35 V for ligand **1b**, −0.78 V and −1.30 V for ligand **1c**, −0.10 V and −1.59 V for ligand **4a**, and −1.10 V and −1.65 V for ligand **4b**. These redox behaviors were attributed to the thioazoformamide/formamide groups present in the ligands [11,21,28]. In metal(II) chlorides, in addition to the peaks attributed to the ligand, quasi-reversible anodic waves and irreversible cathodic waves were observed. In the positive potential range (0 to +1.80 V), the oxidation process corresponds to the M(III)/M(II) redox couple. In the negative potential range (0 to −1.80 V), a reductive process was detected, which is associated with the M(II)/M(I)/M(0) redox transitions.

The cyclic voltammetry analysis of the nickel(II) complexes revealed two irreversible oxidation peaks across the potential range from +0.77 to +1.29 V for all compounds. For complexes **5** and **6**, three quasi-reversible reduction peaks were observed, while complexes **11** and **12** exhibited only one reversible reduction peak. In the case of copper complexes, a

single quasi-reversible oxidation peak was detected from 0.24 to 0.26 V, accompanied by one quasi-reversible and one irreversible reduction peak. The zinc(II) complexes showed an irreversible oxidation peak from 1.21 to 1.46 V, with compounds **13** and **14** featuring one reversible reduction peak, and compounds **7** and **8** presenting three quasi-reversible reduction peaks. Notably, the cyclic voltammetry experiments conducted at different scan rates (100 mV/s, 200 mV/s, and 500 mV/s) demonstrated a proportional increase in peak current with the square root of the scan rate. This observation strongly indicates that the electrode process is controlled by diffusion [29].

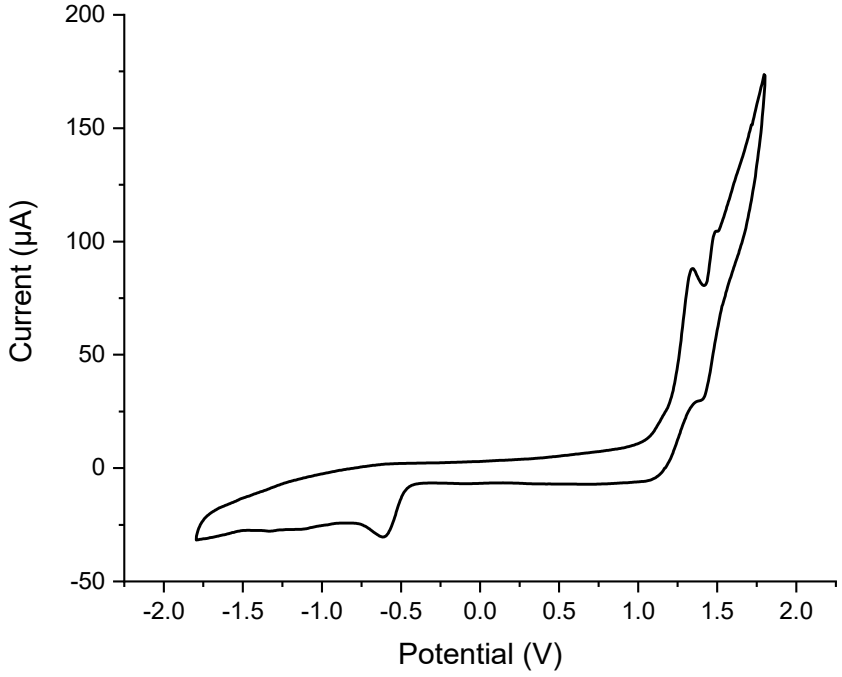


Figure 6. Cyclic voltammetry of complex **14** at 50 mV/s.

3. Experimental

3.1. General Methods

^{1}H NMR experiments were performed on a Bruker AVANCE 500 MHz spectrometer. For ^{1}H NMR, all coupling constants (*J*) are reported in Hz. The multiplicities of the signals are described using the following abbreviations: s = singlet, br s = broad singlet, d = doublet, t = triplet, q = quartet, dd = doublet of doublets, ddd = doublet of doublet of doublets, dq = doublet of quartets, dsep = doublet of septets, tt = triplet of triplets, m = multiplet, and app = apparent. The NMR solvent *d*-chloroform was used and referenced to 7.26 ppm. Infrared spectra were obtained on a Thermo Scientific Nicolet 380 FT-IR spectrometer as thin films on ZnSe disks, and peaks are reported in cm^{-1}. Reaction progress was monitored by thin-layer chromatography on silica gel plates (60-F254), observed under UV light. Elemental analysis was performed on a Vario microcube Elementar Analyzer. Metal (II) salts, $NiCl_2 \cdot 6H_2O$, $CuCl_2$, and $ZnCl_2$ were purchased from Millipore Sigma and used without further purification. For synthesis or analysis, solvents like dichloromethane, acetonitrile, methanol, and hexanes, as well as triethylamine were purchased from ThermoFisher. Reagents for ligand synthesis including 4-methoxyphenylhydrazine, pyrrolidine, and piperidine, were purchased from AK Scientific. Deuterated solvents were purchased from Cambridge Isotopes Laboratory. Carbon disulfide was purchased from Alfa-Aesar.

3.2. General Procedure for Synthesizing Complexes

Ligands were synthesized according to previous reports [11,20]. To synthesize the complex, first, the ligand (ATF or AAF) (0.40 mmol, 1.0 equivalent) was dissolved in 5 mL of solvent (toluene or methanol), then the appropriate amount of metal(II) chloride (0.40 mmol, 1.0 equivalent) was added to the solution. The solution was refluxed for 4 hr and then cooled to room temperature. Precipitates were collected by vacuum filtration and washed with hexane to remove excess ligand. Excess metal (II) chloride was removed by an aqueous workup with complexes dissolved in dichloromethane. After evaporation, the pure complexes were analyzed through ^{1}H NMR (when possible), elemental analysis, and FTIR. Crystals were obtained either by filtration, slow evaporation of solvent, or the slow diffusion of acetonitrile into ether.

$NiCl_2$- pyrrolidine-p-Methoxyphenyl azothioformamide (**5**): Dark red solid, (163 mg) 54%. FTIR (cm^{-1}): 2971, 1576, 1439, 1273, 1010, and 843. Anal Calcd for $C_{24}H_{30}Cl_4N_6O_2S_2Ni_2$: C, 38.04; H, 3.99; N, 11.09. Found: C, 38.12; H, 3.659; N, 11.31.

$NiCl_2$- piperidine-p-Methoxyphenyl azothioformamide (**6**): Dark red solid, (168 mg) 61%. FTIR (cm^{-1}): 2940, 1600, 1449, 1263, 1009, and 851. Anal Calcd for $C_{26}H_{34}Cl_2N_6O_2S_2Ni$: C, 47.58; H, 5.22; N, 12.81. Found: C, 49.12; H, 5.36; N, 13.31.

$ZnCl_2$- pyrrolidine-p-Methoxyphenyl azothioformamide (**7**): Dark red crystals, (192 mg) 63%. ^{1}H NMR (500 MHz, $CDCl_3$) δ 8.50 (br s, 4H), 7.12–7.07 (m, 4H), 4.34 (br s, 4H), 4.11 (br s, 4H), 4.01 (s, 6H), 2.23 (br s, 8H). FTIR (cm^{-1}): 2982, 1573, 1441, 1256, 1007, 843, and 6430. Anal Calcd for $C_{24}H_{30}Cl_4N_6O_2S_2Zn_2$: C, 37.38; H, 3.92; N, 10.90; S, 8.31. Found: C, 37.58; H, 4.038; N, 11.1; S, 8.484.

$ZnCl_2$- piperidine-p-Methoxyphenyl azothioformamide hydrate (**8**): Dark red crystals, (185 mg) 68%. ^{1}H NMR (500 MHz, $CDCl_3$) δ 8.50 (d, *J* = 8.8 Hz, 4H), 7.16–7.08 (m, 4H), 4.50 (br s, 4H), 4.42–4.36 (m, 4H), 4.01 (s, 6H), 2.00 (br s, 4H), 1.90 (p, *J* = 2.7 Hz, 8H). FTIR (cm^{-1}): 2982, 1569, 1446, 1274, 1004, 845, and 631. Anal Calcd for $C_{13}H_{19}Cl_2N_3O_2SZn$: C, 39.09; H, 4.29; N, 10.51; S, 8.02. Found: C, 38.76; H, 4.256; N, 10.43; S, 7.674.

$CuCl_2$- pyrrolidine-p-Methoxyphenyl azothioformamide (**9**): Dark green crystals, (164 mg) 59%. ^{1}H NMR (500 MHz, $CDCl_3$) δ 8.31 (d, *J* = 8.0 Hz, 4H), 7.00 (d, *J* = 8.0 Hz, 4H), 4.31 (br s, 4H), 3.95 (t, *J* = 5.9 Hz, 4H), 3.91 (s, 6H), 2.23 (q, *J* = 9.0 Hz, 8H). FTIR (cm^{-1}): 2982, 1589, 1436, 1265, 1017, 839, and 734. Anal Calcd for $C_{24}H_{30}Cl_2N_6O_2Cu_2S_2$: C, 41.38; H, 4.34; N, 12.06; S, 9.20. Found: C, 41.62; H, 4.346; N, 11.79; S, 9.03.

$CuCl_2$- piperidine-p-Methoxyphenyl azothioformamide (**10**): Dark green crystals, (131 mg) 43%. ^{1}H NMR (500 MHz, $CDCl_3$) δ 8.28 (br s, 4H), 7.36 (br s, 4H), 4.52 (br s, 8H), 3.96 (s, 6H), 2.01 (br d, *J* = 18.2 Hz, 12H). FTIR (cm^{-1}): 2950, 1595, 1437, 1269, 1007, 831, and 706. Anal Calcd for $C_{26}H_{34}Cl_2N_6O_2Cu_2S_2$: C, 43.09; H, 4.73; N, 11.60; S, 8.85. Found: C, 43.59; H, 5.078; N, 11.68; S, 8.793.

$NiCl_2$- pyrrolidine-p-Methoxyphenyl azoformamide (**11**): Yellowish green crystals, (109 mg) 46%. ^{1}H NMR (500 MHz, $CDCl_3$) δ 7.92 (d, *J* = 8.7 Hz, 4H), 6.97 (d, *J* = 8.7 Hz, 4H), 3.87 (s, 6H), 3.68 (t, *J* = 6.5 Hz, 4H), 3.63 (t, *J* = 6.5 Hz, 4H), 2.60–0.95 (m, 8H). FTIR (cm^{-1}): 2943, 1657, 1597, 1464, 1253, and 1011, 854. Anal Calcd for $C_{24}H_{30}Cl_2N_6O_4Ni$: C, 48.36; H, 5.07; N, 14.10. Found: C, 48.50; H, 5.884; N, 13.75.

$NiCl_2$- piperidine-p-Methoxyphenyl azoformamide (**12**): Yellowish green crystals, (156 mg) 63%. ^{1}H NMR (500 MHz, Chloroform-*d*) δ 7.91 (d, *J* = 9.0 Hz, 4H), 6.99 (d, *J* = 9.0 Hz, 4H), 3.89 (s, 6H), 3.74–3.70 (m, 4H,), 3.64–3.60 (m, 4H), 1.72–1.68 (m, 8H), 1.63–1.58 (m, 4H). FTIR (cm^{-1}): 2958, 1684, 1598, 1455, 1235, 1030, and 836. Anal Calcd for $C_{26}H_{34}Cl_2N_6O_4Ni$: C, 50.03; H, 5.49; N, 13.34. Found: C, 50.12; H, 5.559; N, 13.31.

$ZnCl_2$- pyrrolidine-p-Methoxyphenyl azoformamide (**13**): Yellow solid, (229 mg) 74%. ^{1}H NMR (500 MHz, Chloroform-*d*) δ 8.04 (d, *J* = 8.5 Hz, 4H), 7.04 (d, *J* = 7.2 Hz, 4H), 3.92 (s, 6H), 3.76 (dt, *J* = 12.7, 6.0 Hz, 8H), 2.07–1.98 (m, 8H). FTIR (cm^{-1}): 2979, 1647, 1595, 1449,

1267, 1007, 846, and 644. Anal Calcd for $C_{26}H_{33}Cl_4N_7O_4Zn_2$: C, 41.78; H, 4.53; N, 11.69. Found: C, 41.71; H, 4.359; N, 11.77.

$ZnCl_2$- piperidine-p-Methoxyphenyl azoformamide (**14**): Yellow solid, (195 mg) 65%. ^{1}H NMR (500 MHz, $CDCl_3$) δ 8.31 (d, *J* = 9.2 Hz, 4H), 7.11 (d, *J* = 9.2 Hz, 4H), 4.26 (t, *J* = 5.4 Hz, 4H), 4.00 (s, 6H), 3.94 (t, *J* = 5.4 Hz, 4H), 1.86–1.80 (m, 12H). FTIR (cm^{-1}): 2974, 1653, 1599, 1448, 1234, 1006, 850, and 643. Anal Calcd for $C_{26}H_{34}Cl_4N_6O_4Zn_2$: C, 40.71; H, 4.47; N, 10.96. Found: C, 40.99; H, 4.583; N, 10.54.

$CuCl_2$- pyrrolidine-p-Methoxyphenyl azoformamide (**15**): Dark brown crystals, (124 mg) 52%. FTIR (cm^{-1}): 2982, 1655, 1598, 1455, 1231, 1004, 846, and 651. Anal Calcd for $C_{24}H_{30}Cl_2N_6O_4Cu$: C, 47.97; H, 5.03; N, 13.98. Found: C, 47.50; H, 4.884; N, 13.60.

$CuCl_2$- piperidine-p-Methoxyphenyl azoformamide (**16**): Dark brown crystals, (175 mg) 58%. FTIR (cm^{-1}): 2982, 1657, 1599, 1451, 1235, 1014, 852, and 643. Anal Calcd for $C_{26}H_{34}Cl_4N_6O_4Cu_2$: C, 40.90; H, 4.49; N, 11.01. Found: C, 40.22; H, 4.49; N, 10.64.

3.3. X-Ray Diffraction Analysis

Data for complexes **5–11** and **14–16** were collected at 100.00 K on a Bruker D8 VENTURE Duo Fixed Chi Three-Circle Diffractometer using MoK_α radiation (λ = 0.71073 Å). All data were integrated with SAINT V8.40B and corrected for absorption using SADABS 2016/2 [30,31]. The structures were solved by direct methods with SHELXT and refined by full-matrix least-squares methods against F^2 using SHELXL [32,33]. All non-hydrogen atoms were refined with anisotropic displacement parameters. Hydrogen atoms of the investigated structures were located from different Fourier maps but were ultimately placed in geometrically calculated positions and refined using a riding model. Isotropic thermal parameters of the placed hydrogen atoms were fixed to 1.2 times the U value of the atoms they are linked to (1.5 times for methyl groups). Calculations and refinement of the structures were carried out using APEX4 [34] and Olex2 [35] software.

3.4. Electrochemistry

A Pine Research WaveNow potentiostat was used for electrochemical investigations at 25 °C using acetonitrile as solvent and 0.1 M tetrabutylammonium hexafluorophosphate (NBu_4PF_6) as the supporting electrolyte. A three-electrode cell was used in which a glassy carbon (GC) rod was the working electrode, Ag/Ag^+ was the reference electrode and graphite was used as the counter electrode. Cyclic voltammetry was used to characterize the electrochemical behavior of the ligands and their complexes. The scanning potential ranged between −1.8 and 2.0 V (versus Ag/Ag^+) with optimal scan rates of 50 mVs^{-1}. All experiments were performed under an N_2 atmosphere by purging the cell solutions with N_2 gas for approximately 10 min, and the cell solutions were maintained under this atmosphere during the recording of the voltammograms. The glassy carbon electrode was polished with fine alumina powder on a wet polishing cloth for approximately 5 min, then thoroughly washed with distilled water to yield the shiny, mirror-like electrode surface.

3.5. UV–Vis Absorbance

UV–Vis spectroscopic absorption was performed using 5.8×10^{-5} M concentration of each complex in acetonitrile solution through a 1 cm pathlength at 23 °C, scanning wavelengths from 1100 to 190 nm. Each solution was referenced against acetonitrile (solvent) as a blank in a quartz cuvette at room temperature. Absorption experiments were performed in triplicate, and the average of three runs was analyzed and displayed.

4. Conclusions

In this study, the successful synthesis and characterization of 12 Ni(II), Cu(II), and Zn(II) complexes with redox-active arylazothioformamide (ATF) and arylazoformamide

(AAF) ligands containing pyrrolidine and piperidine moieties was shown. Structural analysis by X-ray crystallography revealed diverse coordination modes: Ni(II) complexes showed 2:2 and 1:2 ligand-to-metal ratios for ATF and AAF, respectively, whereas Cu(II) and Zn(II) complexes adopted square planar, distorted tetrahedral, and octahedral geometries. Spectroscopic and electrochemical studies confirmed ligand–metal interactions, as well as a potential reduction in copper(II) to copper(I) during coordination. These findings contribute valuable insights into metal–ligand coordination, with implications for future studies on mixed-metal separations.

Supplementary Materials: The following supporting information can be downloaded at: https://www.mdpi.com/article/10.3390/cryst15100869/s1. General Experimental Methods and X-Ray Diffraction experimental details; Tables S1–S3: X-Ray crystallographic data for complexes **5–16**; Figure S1: (A) Hirshfeld surface analysis, (B) Hirshfeld surface to visualize intermolecular interaction and (C) fingerprint plot of major contact in compounds **6–16**; Figures S2–S9: ^{1}H NMR of complexes **7–14;** Table S4 FTIR data for ligands **1b,1c, 4a, 4b** and complexes **5–16**; Figure S10–S13: Cyclic Voltammetry data for various complexes **6–16**; Figure S14–S15: UV-VIS absorbance for complexes **5,6,11,12** and **7,8,13,14**.

Author Contributions: Conceptualization, K.V.W.; Methodology, L.T. and K.V.W.; Validation, J.N.; Formal analysis, L.T., J.N. and K.V.W.; Investigation, L.T.; Data curation, J.N.; Writing—original draft, L.T.; Writing—review & editing, J.N. and K.V.W.; Project administration, K.V.W.; Funding acquisition, K.V.W. All authors have read and agreed to the published version of the manuscript.

Funding: This research was funded by U.S. National Science Foundation, grant number are 2350243 and 1337908, and National Institutes of Health, grant number is 1P30GM103546-2.

Data Availability Statement: The original contributions presented in this study are included in the article/Supplementary Materials. Further inquiries can be directed to the corresponding author.

Acknowledgments: X-ray crystallographic data were collected at the University of Montana X-ray diffraction core facility supported by the Center for Biomolecular Structure and Dynamics CoBRE (National Institutes of Health, CoBRE NIGMS P30GM103546). Single crystal X-ray diffraction data were collected using a Bruker D8 Venture, principally supported by NSF MRI CHE-1337908. This work was also supported, in part, by NSF CAS-SC Award 2350243.

Conflicts of Interest: The authors declare no conflict of interest.

References

1. Franz, K.J.; Metzler-Nolte, N. Introduction: Metals in Medicine. *Chem. Rev.* **2019**, *119*, 727–729. [CrossRef] [PubMed]
2. Zhang, C.X.; Lippard, S.J. New Metal Complexes as Potential Therapeutics. *Curr. Opin. Chem. Biol.* **2003**, *7*, 481–489. [CrossRef] [PubMed]
3. Ndagi, U.; Mhlongo, N.; Soliman, M. Metal Complexes in Cancer Therapy—An Update from Drug Design Perspective. *Drug Des. Devel. Ther.* **2017**, *11*, 599–616. [CrossRef]
4. Jacobs, A.; Renaudin, G.; Forestier, C.; Nedelec, J.-M.; Descamps, S. Biological Properties of Copper-Doped Biomaterials for Orthopedic Applications: A Review of Antibacterial, Angiogenic and Osteogenic Aspects. *Acta Biomater.* **2020**, *117*, 21–39. [CrossRef]
5. Sakthivel, R.V.; Sankudevan, P.; Vennila, P.; Venkatesh, G.; Kaya, S.; Serdaroğlu, G. Experimental and Theoretical Analysis of Molecular Structure, Vibrational Spectra and Biological Properties of the New Co(II), Ni(II) and Cu(II) Schiff Base Metal Complexes. *J. Mol. Struct.* **2021**, *1233*, 130097. [CrossRef]
6. Yang, P.; Chen, H.; Wang, Z.-Z.; Zhang, L.-L.; Zhang, D.-D.; Shi, Q.-S.; Xie, X.-B. Crystal Structures and Biological Properties of Aroylhydrazone Ni(II) Complexes. *J. Inorg. Biochem.* **2020**, *213*, 111248. [CrossRef]
7. Osowole, A.A.; Kolawole, G.A.; Fagade, O.E. Synthesis, Physicochemical, and Biological Properties of Nickel(II), Copper(II), and Zinc(II) Complexes of an Unsymmetrical Tetradentate Schiff Base and Their Adducts. *Synth. React. Inorg. Met. Org. Nano-Met. Chem.* **2005**, *35*, 829–836. [CrossRef]
8. Takaya, J. Catalysis Using Transition Metal Complexes Featuring Main Group Metal and Metalloid Compounds as Supporting Ligands. *Chem. Sci.* **2021**, *12*, 1964–1981. [CrossRef]

9. Tsuji, J. *Transition Metal Reagents and Catalysts: Innovations in Organic Synthesis*; John Wiley & Sons: Hoboken, NJ, USA, 2002.
10. Obeso, J.L.; Huxley, M.T.; Leyva, C.; Gabriel Flores, J.; Martín-Guaregua, N.; Viniegra, M.; Aguilar-Pliego, J.; Antonio De Los Reyes, J.; Ibarra, I.A.; Peralta, R.A. The Role of Dynamic Metal-Ligand Bonds in Metal-Organic Framework Chemistry. *Coord. Chem. Rev.* **2023**, *496*, 215403. [CrossRef]
11. Tiwari, L.; Leach, C.; Williams, A.; Lighter, B.; Heiden, Z.; Roll, M.F.; Moberly, J.G.; Cornell, K.A.; Waynant, K.V. Binding Mechanisms and Therapeutic Activity of Heterocyclic Substituted Arylazothioformamide Ligands and Their Cu(I) Coordination Complexes. *ACS Omega* **2024**, *9*, 37141–37154. [CrossRef]
12. Bechgaard, K.; Woldbye, F.; Lindeløv, F.; Østvold, T.; Bjørseth, A.; Powell, D.L. Nonplanar Electron Transfer Complexes. I. The Chemistry of Five Ni-N2S2z Complexes Derived from Nickel-Bis-N,N-Diethylphenylazothioformamide. *Acta Chem. Scand.* **1974**, *28*, 185–193. [CrossRef]
13. Bechgaard, K.; Borggaard, O.K.; Tuhtar, D.; Pouchard, M.; Hagenmuller, P.; Andresen, A.F. Nonplanar Electron Transfer Complexes. II. The Chemistry of Four Cu--N2S2z Complexes Derived from Copper-Bis-N,N-Diethylphenylazothioformamide. *Acta Chem. Scand.* **1977**, *31*, 683–688. [CrossRef]
14. Jensen, K.A.; Bechgaard, K.; Pedersen, C.T.; Pearson, W.B. Coordination Compounds of Phenylazothioformamides. *Acta Chem. Scand.* **1968**, *22*, 3341–3342. [CrossRef]
15. Nielsen, K.; Bechgaard, K.; Krebs, F. Effective Removal and Quantitative Analysis of Pd, Cu, Ni, and Pt Catalysts from Small-Molecule Products. *Synthesis* **2006**, *2006*, 1639–1644. [CrossRef]
16. Nielsen, K.T.; Bechgaard, K.; Krebs, F.C. Removal of Palladium Nanoparticles from Polymer Materials. *Macromolecules* **2005**, *38*, 658–659. [CrossRef]
17. Tiwari, L.; Hulley, E.B.; Waynant, K.V. Investigating Arylazoformamide Ligands in Palladium(II) Precatalysts through the Suzuki–Miyaura Cross-Coupling Reaction. *J. Org. Chem.* **2024**, *89*, 17917–17925. [CrossRef] [PubMed]
18. Tiwari, L.; Chavez, K.; Hulley, E.B.; Waynant, K.V. Synthetic and Mechanistic Evaluation of Palladium(II) Bis(Arylazoformamide) Precatalysts in the Sonogashira Reaction. *Organometallics* **2025**, *44*, 1530–1537. [CrossRef]
19. Hirose, D.; Gazvoda, M.; Košmrlj, J.; Taniguchi, T. Systematic Evaluation of 2-Arylazocarboxylates and 2-Arylazocarboxamides as Mitsunobu Reagents. *J. Org. Chem.* **2018**, *83*, 4712–4729. [CrossRef]
20. Tiwari, L.; Waynant, K.V. The Synthesis and Structural Properties of a Chloridobis{*N*-[(4-Methoxyphenyl)Imino]Pyrrolidine-1-Carboxamide}zinc(II) (Acetonitrile)Trichloridozincate Coordination Complex. *Acta Crystallogr. Sect. E Crystallogr. Commun.* **2024**, *80*, 14–17. [CrossRef]
21. Tiwari, L.; Heiden, Z.M.; Waynant, K.V. Exploring the Electronic Influence on Coordination Complexes Formed from Appended Pyrrolidine Azothioformamide Ligands and Copper(I) Salts. *J. Mol. Struct.* **2025**, *1320*, 139740. [CrossRef]
22. Pradhan, R.; Groner, V.M.; Gutman, K.L.; Larson, G.E.; Kan, Y.; Zhang, Q.; Heiden, Z.M.; Roll, M.F.; Moberly, J.G.; Waynant, K.V. Evaluating Coordinative Binding Mechanisms through Experimental and Computational Studies of Methoxy-Substituted Arylazothioformamide Copper(I) Complexes. *Eur. J. Inorg. Chem.* **2022**, *2022*, e202200421. [CrossRef]
23. Johnson, N.A.; Wolfe, S.R.; Kabir, H.; Andrade, G.A.; Yap, G.P.A.; Heiden, Z.M.; Moberly, J.G.; Roll, M.F.; Waynant, K.V. Deconvoluting the Innocent vs. Non-Innocent Behavior of N,N-Diethylphenylazothioformamide Ligands with Copper Sources. *Eur. J. Inorg. Chem.* **2017**, *2017*, 5576–5581. [CrossRef]
24. Spackman, P.R.; Turner, M.J.; McKinnon, J.J.; Wolff, S.K.; Grimwood, D.J.; Jayatilaka, D.; Spackman, M.A. *CrystalExplorer*: A Program for Hirshfeld Surface Analysis, Visualization and Quantitative Analysis of Molecular Crystals. *J. Appl. Crystallogr.* **2021**, *54*, 1006–1011. [CrossRef]
25. Low, M.L.; Paulus, G.; Dorlet, P.; Guillot, R.; Rosli, R.; Delsuc, N.; Crouse, K.A.; Policar, C. Synthesis, Characterization and Biological Activity of Cu(II), Zn(II) and Re(I) Complexes Derived from S-Benzyldithiocarbazate and 3-Acetylcoumarin. *BioMetals* **2015**, *28*, 553–566. [CrossRef]
26. Konstantinović, S.S.; Radovanović, B.C.; Krklješ, A. Thermal Behaviour of Co(II), Ni(II), Cu(II), Zn(II), Hg(II) and Pd(II) Complexes with Isatin-β-Thiosemicarbazone. *J. Therm. Anal. Calorim.* **2007**, *90*, 525–531. [CrossRef]
27. Connelly, N.G.; Geiger, W.E. Chemical Redox Agents for Organometallic Chemistry. *Chem. Rev.* **1996**, *96*, 877–910. [CrossRef] [PubMed]
28. Pasini, A.; Bernini, E.; Scaglia, M.; De Santis, G. Studies on the Oxidation of CuII Complexes of Quadridentate Schiff Bases Derived from Salicylaldehyde or Ortho-Aminophenol. *Polyhedron* **1996**, *15*, 4461–4467. [CrossRef]
29. Kulkarni, A.D.; Patil, S.A.; Badami, P.S. Electrochemical Properties of Some Transition Metal Complexes: Synthesis, Characterization and In-Vitro Antimicrobial Studies of Co(II), Ni(II), Cu(II), Mn(II) and Fe(III) Complexes. *Int. J. Electrochem. Sci.* **2009**, *4*, 717–729. [CrossRef]
30. Bruker AXS Inc. *SAINT, V8.40B*; Bruker AXS Inc.: Madison, WI, USA, 2003.
31. Krause, L.; Herbst-Irmer, R.; Sheldrick, G.M.; Stalke, D. Comparison of Silver and Molybdenum Microfocus X-Ray Sources for Single-Crystal Structure Determination. *J. Appl. Crystallogr.* **2015**, *48*, 3–10. [CrossRef]

32. Sheldrick, G.M. *SHELXT*—Integrated Space-Group and Crystal-Structure Determination. *Acta Crystallogr. Sect. Found. Adv.* **2015**, *71*, 3–8. [CrossRef]
33. Sheldrick, G.M. Crystal Structure Refinement with *SHELXL*. *Acta Crystallogr. Sect. C Struct. Chem.* **2015**, *71*, 3–8. [CrossRef]
34. Bruker AXS Inc. *APEX4*; Bruker AXS Inc.: Madison, WI, USA, 2021.
35. Dolomanov, O.V.; Bourhis, L.J.; Gildea, R.J.; Howard, J.A.K.; Puschmann, H. *OLEX2*: A Complete Structure Solution, Refinement and Analysis Program. *J. Appl. Crystallogr.* **2009**, *42*, 339–341. [CrossRef]

Disclaimer/Publisher's Note: The statements, opinions and data contained in all publications are solely those of the individual author(s) and contributor(s) and not of MDPI and/or the editor(s). MDPI and/or the editor(s) disclaim responsibility for any injury to people or property resulting from any ideas, methods, instructions or products referred to in the content.